

Preferred Features of a Fluorine-19 MRI Probe for Amyloid Detection in the Brain

Daijiro Yanagisawa^a, Hiroyasu Taguchi^a, Nor Faeizah Ibrahim^a, Shigehiro Morikawa^b, Akihiko Shiino^b, Toshiro Inubushi^b, Koichi Hirao^c, Nobuaki Shirai^c, Takayuki Sogabe^d and Ikuo Tooyama^{a,*}

^aMolecular Neuroscience Research Center, Shiga University of Medical Science, Seta Tsukinowa-cho, Otsu, Japan

^bBiomedical MR Science Center, Shiga University of Medical Science, Seta Tsukinowa-cho, Otsu, Japan

^cNortheastern Industrial Research Center of Shiga Prefecture, Nagahama, Japan

^dOtsuka Pharmaceutical Co., Ltd, Kawauchi-cho, Japan

Handling Associate Editor: Shun Shimohama

Accepted 2 October 2013

Abstract. Fluorine-19 magnetic resonance imaging (¹⁹F MRI) could be a promising approach for imaging amyloid deposition in the brain. However, the required features of a ¹⁹F MRI probe for amyloid detection remain unclear. In the present study, we investigated a series of compounds as potent ¹⁹F probes that could prevent the reduction in MR signal when bound to amyloid plaques in the brain. Each compound consists of styrylbenzoxazole as a core structure linked by a different length of polyethylene glycol (PEG) chain to one of three types of fluorine-labeled group: a trifluoroethoxy group, a hexafluoroisopropoxy group, or a 3',5'-bis(trifluoromethyl)benzylamino group. Among these compounds, 6-(3',6',9',15',18',21'-hepta-oxa-23',23',23'-trifluorotricosanyloxy)-2-(4'-dimethylaminostyryl)benzoxazole [compound 3b (m = 6)], which has a trifluoroethoxy group with seven ethylene glycol groups in the PEG chain, showed significant ¹⁹F MR signals in the brains of A β PPswe/PS1dE9 double-transgenic mice, but not wild-type mice. This suggested that compound 3b (m = 6) could be a useful ¹⁹F MRI probe for amyloid detection. Furthermore, this study identified the most effective length of PEG chain between the fluorine-labeled group and the core structure to ensure a strong MR signal when the probe is bound to amyloid plaques.

Keywords: Alzheimer's disease, amyloid deposition, amyloid imaging, fluorine-19 MRI, magnetic resonance imaging

INTRODUCTION

Alzheimer's disease (AD) is characterized by a progression from episodic memory problems to a slow global decline in cognitive function [1, 2]. The pathological features of AD include the formation of senile plaques composed of extracellular deposits of

amyloid- β (A β) and neurofibrillary tangles formed by the intracellular accumulation of abnormally hyperphosphorylated tau. Recent evidence concerning the progression of AD strongly supports the amyloid cascade hypothesis in which a pathological change of A β in the brain is an initiating event [3, 4]. Deposition of A β occurs many years before clinical symptoms appear. After a lag period, neurofibrillary tangle formation and neuronal loss become abnormal, leading to cognitive impairment. Accordingly, estimating the level of A β deposition in the brain would be informative for early diagnosis of AD and for evaluating AD progression. Furthermore, such a measure could help to

*Correspondence to: Ikuo Tooyama, M.D., Ph.D., Molecular Neuroscience Research Center, Shiga University of Medical Science, Seta Tsukinowa-cho, Otsu 520-2192, Japan. Tel.: +81 77 548 2330; Fax: +81 77 548 2331; E-mail: kinchan@belle.shiga-med.ac.jp.

find asymptomatic individuals at the preclinical stage of AD [5].

Noninvasive imaging methods to visualize A β deposition in the brain, such as positron emission tomography (PET), have recently attracted much attention. Magnetic resonance imaging (MRI) is another promising modality for amyloid imaging, and several novel contrast agents and pulse sequences for the detection of amyloid deposition using MRI have been reported [6–17]. Indeed, we have developed novel fluorine-19 (^{19}F)-labeled contrast agents for the detection of amyloid deposition using ^{19}F MRI [18–20]. The advantages of ^{19}F MRI are as follows: MR sensitivity of ^{19}F is relatively high compared to the sensitivity of various nuclei other than ^1H (^1H , 100%; ^{19}F , 83%; ^{31}P , 6.6%; ^{13}C , 1.6%); no ^{19}F atoms exist in biological tissues, thus producing low endogenous background noise; and, the ^{19}F atom is a non-radioactive isotope, with 100% natural abundance. Accordingly, ^{19}F MRI would be a highly sensitive, easily available, low-background, and cost-effective approach for detecting A β deposition once a suitable high-quality probe is developed. However, the preferred features of a probe used for amyloid imaging with ^{19}F MRI are still unclear. Our previous study demonstrated that highly hydrophobic probes might be trapped by the lipid components of the brain such as myelin, thus inhibiting molecule mobility, causing shortening of T_2 and broadening of the MR signal, and in turn a reduction in MR signal [18]. This reduction in MR signal is induced when the probe binds to amyloid plaques in the brain [18, 20]. Accordingly, a method to regulate the hydrophilicity/hydrophobicity of the probe and thus avoid the reduction in MR signal when the probe is bound to amyloid plaques is a key factor in the development of a high-quality ^{19}F MRI probe for amyloid imaging.

In the present study we investigated a series of compounds as potent ^{19}F probes that may generate strong MR signals when bound to amyloid plaques in the brain. The probes consist of a core structure linked to a different fluorine-labeled group by a specific length of polyethylene glycol (PEG) chain (from 2 to 12 ethylene glycol units). The fluorine labels examined belong to one of three types of trifluoromethyl groups: a single trifluoromethyl group (3b, 5b), two equivalent trifluoromethyl groups attached to an aliphatic carbon atom (3c, 5c), and two equivalent trifluoromethyl groups attached to an aromatic ring carbon (3a, 5a). The aim of the study was to determine the optimum length of PEG chain to link with the appropriate fluorine-labeled group to generate a probe capable of detecting amyloid deposition in the brain with ^{19}F MRI.

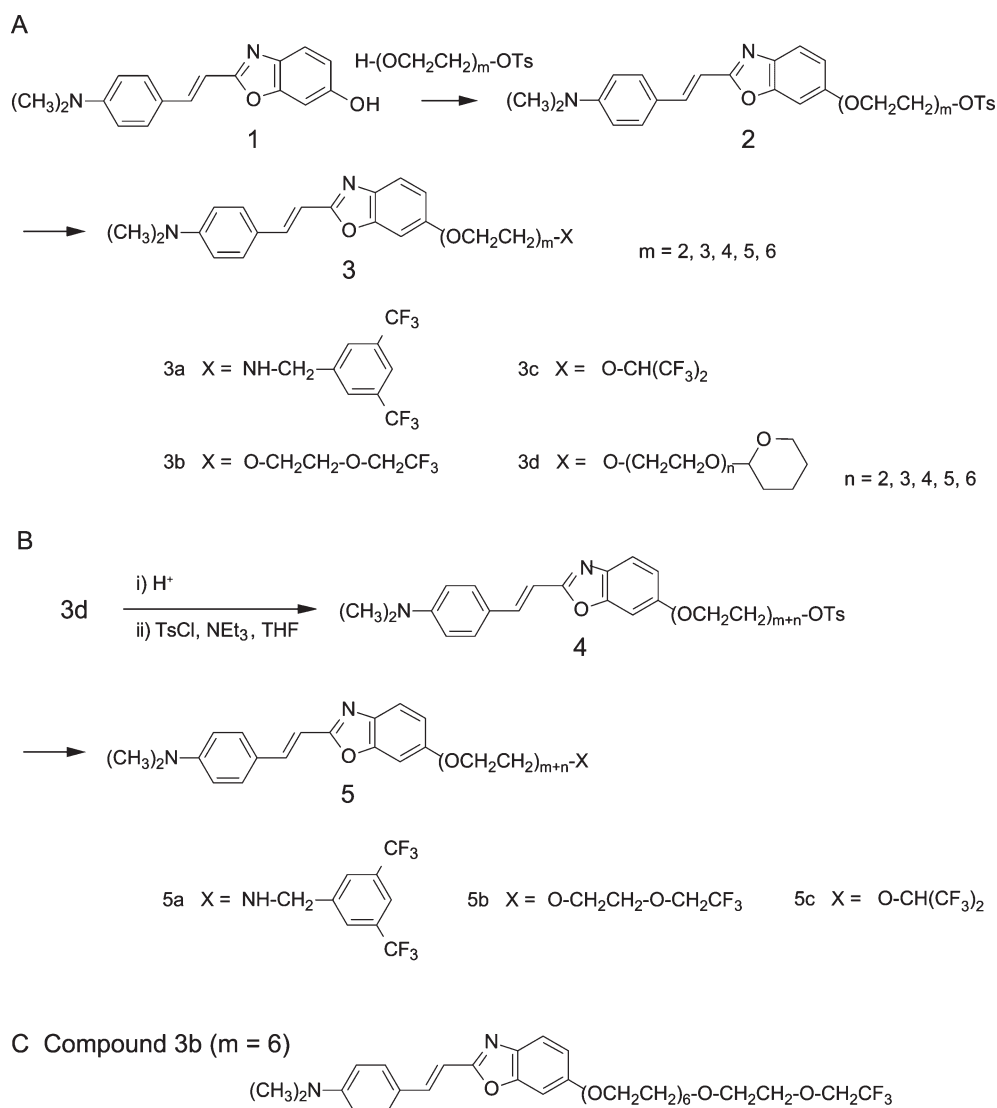
MATERIALS AND METHODS

Synthesis

We synthesized a series of compounds as potent ^{19}F MRI probes. They were fluorescent chemicals, and each compound consisted of styrylbenzoxazole as a core structure linked to a different fluorine-labeled group by a different length of PEG chain. The synthetic pathways are depicted in the Supplementary Materials and Methods, and Supplementary Table 1. In brief, styrylbenzoxazoles with fluorine substituents (compounds 3 and 5) were prepared according to a previously reported procedure [18]. Thus, compound 2 probes ($m=2\sim 6$) were made from 6-hydroxy-2-(4'-dimethylaminostyryl)benzoxazole (compound 1) by a Mitsunobu reaction. The preparation procedure for compound 3 is summarized in Scheme 1A. Reaction of compound 2 with benzylamine derivatives in dimethyl sulfoxide produced the benzylamino derivative 3a with fluorine substituents. Compounds 3b to 3d were made by substitution of the tosyloxy group with alkoxides prepared from the appropriate alcohol and sodium hydride in tetrahydrofuran or N,N-dimethylformamide. The fluorine derivatives with longer PEG chains (compound 5, $m+n=7\sim 12$) were prepared from compound 3d as shown in Scheme 1B. The deprotection of the tetrahydropyranyl group of compound 3d with hydrochloric acid in ethanol gave the corresponding alcohols, which were readily tosylated to produce compound 4. For compounds with a benzylamine derivative or alkoxide, a substitution reaction of the tosyloxy group was performed in a similar manner to that for compound 3. The values of molecular mass and ClogP of the compounds synthesized in the present study are listed in Table 1.

Table 1
Molecular masses and ClogP values for the synthesized compounds

Name	Molecular mass	ClogP
3a ($m=2$)	637.61	6.77
3a ($m=3$)	681.66	6.61
3a ($m=4$)	725.72	6.46
3a ($m=5$)	769.77	6.30
3b ($m=2$)	494.50	4.39
3b ($m=4$)	582.61	4.08
3b ($m=5$)	626.66	3.93
3b ($m=6$)	670.71	3.77
5b ($m+n=7$)	714.77	3.62
5b ($m+n=8$)	758.82	3.46
5b ($m+n=10$)	846.92	3.15
5b ($m+n=12$)	935.03	2.84
3c ($m=2$)	518.45	5.51
3c ($m=6$)	694.66	4.89
5c ($m+n=8$)	782.76	4.58



Scheme 1. Synthesis and structures of styrylbenzoxazole derivatives. The numbers 'm' and 'm + n' express the length of the polyethylene glycol (PEG) chain. The compounds bearing shorter chains ($m \leq 6$) belong to 'compound 3' and those bearing longer ones ($m + n \geq 7$) belong to 'compound 5'. The groups 'a', 'b' and 'c' express the type of trifluoromethyl groups attached to the PEG chain. Compounds 3a and 5a contain a 3,5-bis(trifluoromethyl)benzylamino group, compounds 3b and 5b contain a 2,2,2-trifluoroethoxy group, and compounds 3c and 5c contain a hexafluoroisopropoxy group.

Animals

$\text{A}\beta\text{PP}^{\text{swe}}/\text{PS1}^{\text{dE9}}$ double-transgenic ($\text{A}\beta\text{PP}/\text{PS1}$) mice with a C57BL/6 background were obtained from Jackson Laboratory (Bar Harbor, ME). The $\text{A}\beta\text{PP}/\text{PS1}$ mice express a chimeric mouse/human amyloid- β protein precursor ($\text{A}\beta\text{PP}$) with mutations K594N and M595L linked to Swedish familial AD (Mo/Hu $\text{A}\beta\text{PP}^{\text{695swe}}$), and human presenilin 1 (PS1) carrying the exon-9-deleted variant associated with familial AD (PS1dE9) [21]. Two transgenes are

inserted at a single locus, and each is controlled by an independent mouse prion promoter element, directing transgene expression predominantly to central nervous system neurons [21]. Heterozygous males were bred with wild-type C57BL/6 females (purchased from Jackson Laboratory). Offspring were ear punched and genotyped using polymerase chain reaction. Mice not expressing the transgene were used as wild-type controls. Mice were maintained in standard laboratory cages at 23°C under a 12-h light/dark cycle (lights on at 08:00–20:00) with free access to water and food. All

experimental procedures in this study were approved by the Committee on Animal Care of Shiga University of Medical Science.

Magnetic resonance imaging

We used a 7.0 T horizontal-bore MR scanner (Unity Inova; Agilent Technologies, Santa Clara, CA) [18, 20]. A home-built circular-type surface coil measuring 1.6 cm in diameter and tuned to both the ^1H and ^{19}F frequencies (300 MHz and 282 MHz, respectively) was used to collect the data. Compounds were dissolved at 10 mg/ml in saline containing 10% Cremophor EL or 10% Tween 80 before use. Mice, under anesthesia with sodium pentobarbital (50 mg/kg, i.p.; Dainippon Sumitomo Pharma, Osaka, Japan), were intravenously injected with compounds at a dose of 200 mg/kg via the tail vein over a 100-min period by continuous infusion at a rate of 0.2 ml/kg/min. Immediately after the injection, the mice were placed in the MR scanner and general anesthesia was maintained with intermittent infusion of sodium pentobarbital through a polyethylene tube inserted intraperitoneally. Additional dosage of sodium pentobarbital for maintaining anesthesia was determined by monitoring respiratory rate. The animals were warmed with an air drier and rectal temperature was monitored throughout the experiments. We also measured MR in mice that were killed by an overdose of sodium pentobarbital (200 mg/kg, i.p.) at indicated time periods after injection of the compounds.

^1H gradient-echo magnetic resonance imaging

^1H gradient-echo MR images of the mouse brain were obtained with 150-ms repetition time (TR), 3-ms echo time, 60° flip angle, 1.5-mm slice thickness, 24 mm \times 24 mm field of view, and 128 \times 128 resolution.

^{19}F magnetic resonance measurement

A nonlocalized ^{19}F nuclear magnetic resonance (NMR) spectrum was obtained from the whole head using a single pulse sequence with 8192 data points, 40,000-Hz spectral width, 1-s TR, and 600 acquisitions (for 10 min).

Free induction decay data of ^{19}F chemical shift imaging (^{19}F CSI) were collected with a 40,000-Hz spectral width, 24 mm \times 24 mm field of view in the horizontal and sagittal planes, 1-s TR, 200- μs phase encoding time, and 68 acquisitions for each central

44 phase-encoding step out of 8×8 steps. For the residual 20 phase-encoding steps in the periphery of k-space, zero data were used. The total acquisition time for one data set was 50 min. A slice-selective pulse was not used, but slice selection was achieved by the sensitivity of the radio frequency (RF) coil in the case of the horizontal plane. Whole signals covered by the coil sensitivity were acquired. The raw data were processed by 3D-Fourier transformation with 40-Hz line broadening and zero filling, and then finally converted to 32×32 spectral data sets. The ^{19}F image was constructed by integrating the ^{19}F signal intensities of compound peaks in individual pixels. We did not determine the flip angle of the excitation pulse for ^{19}F . The RF power was optimized to obtain the maximal ^{19}F signal intensity with 1-s TR using a compound-containing phantom and animals. The optimized RF power was used for both the ^{19}F single pulse and ^{19}F CSI sequences.

Semi-quantitative analysis of ^{19}F MR signal intensity in the brain region

The signal intensity of ^{19}F MR images with matrix size 256 \times 256 pixels was quantified with image processing software (Image J; National Institutes of Health, Bethesda, MD). Sixteen regions of interest (ROIs), with a square area of 64 pixels each, were placed evenly over the forebrain region of the ^{19}F MR images. Then, mean density in the ROIs in the forebrain was measured. At the same time, mean background density was measured using 16 ROIs placed over a region where there was no tissue. Finally, the values of ^{19}F MR signal intensity for the forebrain region were obtained by subtracting the background values from the forebrain values in each image.

Immunohistochemistry

Mice were sacrificed under deep anesthesia with sodium pentobarbital (50 mg/kg, i.p.). The brain was removed quickly from each mouse, post-fixed in 4% paraformaldehyde for 24 h at 4°C , and then immersed in 0.1 M phosphate buffer (pH 7.4) containing 15% sucrose and 0.1% sodium azide for at least 2 days for cryoprotection. We did not perfuse the brain before collection in the present study, unless otherwise specified. The brains were cut into 20- μm sections in a cryostat. Free-floating sections were treated with 0.3% hydrogen peroxide in 0.1 M phosphate-buffered saline (PBS) containing 0.3% Triton X-100 (PBS-T, pH 7.4) to eliminate endogenous peroxidase activity. After

several washes, the sections were treated with 2% bovine serum albumin (BSA) in PBS-T for 30 min at room temperature to block non-specific protein binding. The sections were then incubated with rabbit polyclonal antibody against the N-terminal of human A β (1:500; Immuno-Biological Laboratories, Takasaki, Japan) in PBS-T containing 0.2% BSA for 24 h at 4°C, followed by biotinylated anti-rabbit IgG (1:1,000; Vector Laboratories, Burlingame, CA) for 1 h at room temperature. The sections were then incubated with avidin-biotin-peroxidase complex (Vectastain ABC Elite kit, 1:3,000; Vector Laboratories) for 1 h at room temperature. All of the sections were washed several times with PBS-T between steps, and labeling was then revealed by 3,3'-diaminobenzidine (DAB; Dojindo Laboratories, Kumamoto, Japan), with nickel ammonium, which yielded a dark blue color. The sections were then mounted on glass slides and coverslipped with Entellan new (Merck Millipore, Billerica, MA).

For fluorescence microscopy, free-floating sections were treated with 2% BSA in PBS-T for 30 min at room temperature to block non-specific protein binding. The sections were then incubated overnight at 4°C with rabbit polyclonal antibody against the N-terminal of human A β (1:500) in PBS-T containing 0.2% BSA, followed by Alexa Fluor 555-conjugated anti-rabbit IgG antibody (1:500; Invitrogen, Carlsbad, CA) in PBS-T for approximately 4 h at room temperature. All of the sections were washed several times with PBS-T between steps. The sections were mounted on glass slides and coverslipped with Immu-Mount (Thermo, Pittsburgh, PA) for subsequent observation by fluorescence microscopy (BZ-8100; Keyence, Osaka, Japan) using a DAPI-BP filter (excitation filter 340–380 nm; dichroic mirror 400 nm; emission filter 435–485 nm) for fluorescence from the compounds and a Texas Red filter (excitation filter 540–580 nm; dichroic mirror 595 nm; emission filter 600–660 nm) to visualize the anti-A β antibody binding.

Labeling with compound 3b (m = 6) in human AD brain sections

All experiments using human materials were approved by and performed in accordance with the guidelines of the Ethics Committees of Shiga University of Medical Science, and informed consent was obtained from the patients' guardians. Postmortem dissected brain blocks fixed with formalin were cut into 20- μm sections. Compound 3b (m = 6) was dissolved at 2 mg/ml in dimethyl sulfoxide and the solution was then diluted to 50 $\mu\text{g}/\text{ml}$ in PBS-T. The temporal lobe

sections of AD brain were immersed in 50 $\mu\text{g}/\text{ml}$ of compound 3b (m = 6) for 1 h at room temperature. The sections were then incubated with mouse monoclonal antibodies against A β (6E10; 1:1,000; Covance, Princeton, NJ) or tau phosphorylated at S202 and T205 (AT8; 1:2,000; Thermo) overnight at 4°C, followed by Alexa Fluor 647-conjugated anti-mouse IgG antibody (1:500; Invitrogen) for 4 h at room temperature. All antibodies were diluted in PBS-T, and sections were washed with PBS-T after each step. Stained sections were observed by fluorescence microscopy (BZ-8100).

Statistical analysis

Data are presented as mean \pm standard error of the mean (S.E.M.). The statistical significance between two groups was analyzed by the Mann-Whitney test (GraphPad Prism; GraphPad Software, La Jolla, CA).

RESULTS

Comparison of ^{19}F MR signal of compounds in the mouse brain

First of all, it was important for us to determine the best length of PEG chain for linking the fluorine-labeled group with the core structure. To compare ^{19}F MR signals between brains with and without amyloid deposition, A β PP/PS1 and wild-type mice aged 16 to 18 months were injected intravenously with the different compounds at a dose of 200 mg/kg, and then euthanized 3 h after the end of the injection. Subsequently, ^{19}F MRI was measured in the mouse head in the sagittal plane for 300 min. We used one wild-type mouse and one A β PP/PS1 mouse in each cohort.

Initially, we investigated the ^{19}F MR signals of the compounds containing a single trifluoromethyl group in the molecule (3 fluorine atoms; type b): compounds 3b (m = 4), 3b (m = 5), 3b (m = 6), 5b (m + n = 7), 5b (m + n = 8), 5b (m + n = 10), and 5b (m + n = 12), all of which have a trifluoroethoxy group with 5, 6, 7, 8, 9, 11, and 13 ethylene glycol groups in the PEG chain, respectively. We generally used 10% Tween 80 to solubilize the compounds, but for compounds 3b (m = 4) and 3b (m = 5), 10% Cremophor EL was used, because these compounds did not dissolve in 10% Tween 80.

Compounds 3b (m = 4) and 3b (m = 5) showed a moderate level of ^{19}F MR signal in the forebrain and a strong signal in the cerebellum of A β PP/PS1 mice, while no signal was detected in the forebrain of wild-type mice (Fig. 1). Compound 3b (m = 6) showed a stronger ^{19}F MR signal in the entire brain

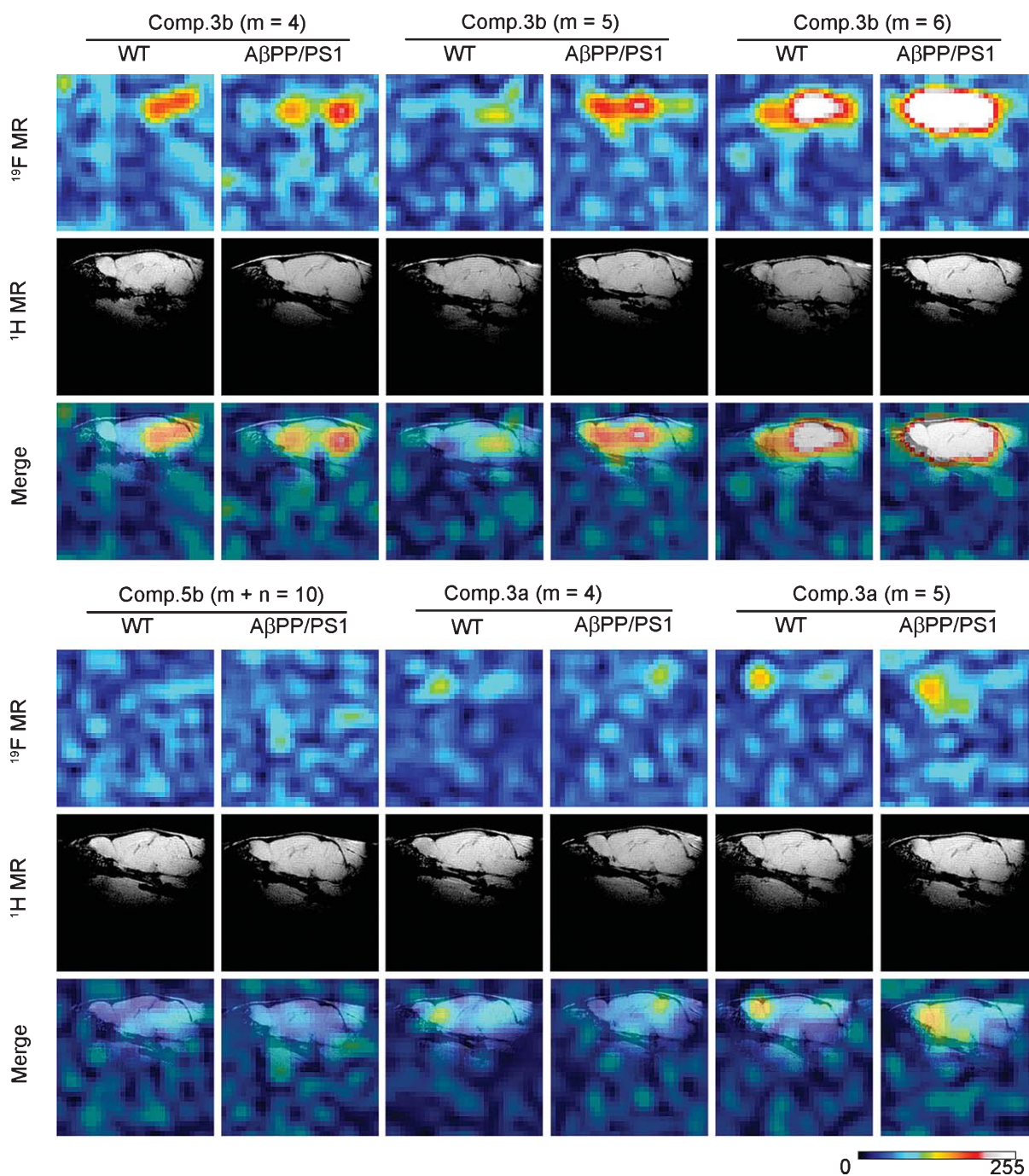


Fig. 1. Differences in fluorine-19 magnetic resonance (^{19}F MR) signals in 16- to 18-month-old wild-type (WT) and A β PPswe/PS1dE9 double-transgenic (A β PP/PS1) mice that were injected with probes prepared in the present study. Mice were euthanized 3 h after the injection of probes. Subsequently, ^{19}F MR images were measured for 300 min in the sagittal plane.

of both A β PP/PS1 and wild-type mice when it was dissolved in 10% Cremophor EL (Fig. 1). On the other hand, when compound 3b (m=6) was dissolved in 10% Tween 80, a strong ^{19}F MR signal

was detected in the brain of A β PP/PS1 mice, whereas the ^{19}F MR signal became weak in wild-type mice (Fig. 2A; 3 h). ^{19}F MR data in mice injected with compound 3b (m=7) and compound 3b (m=8) were

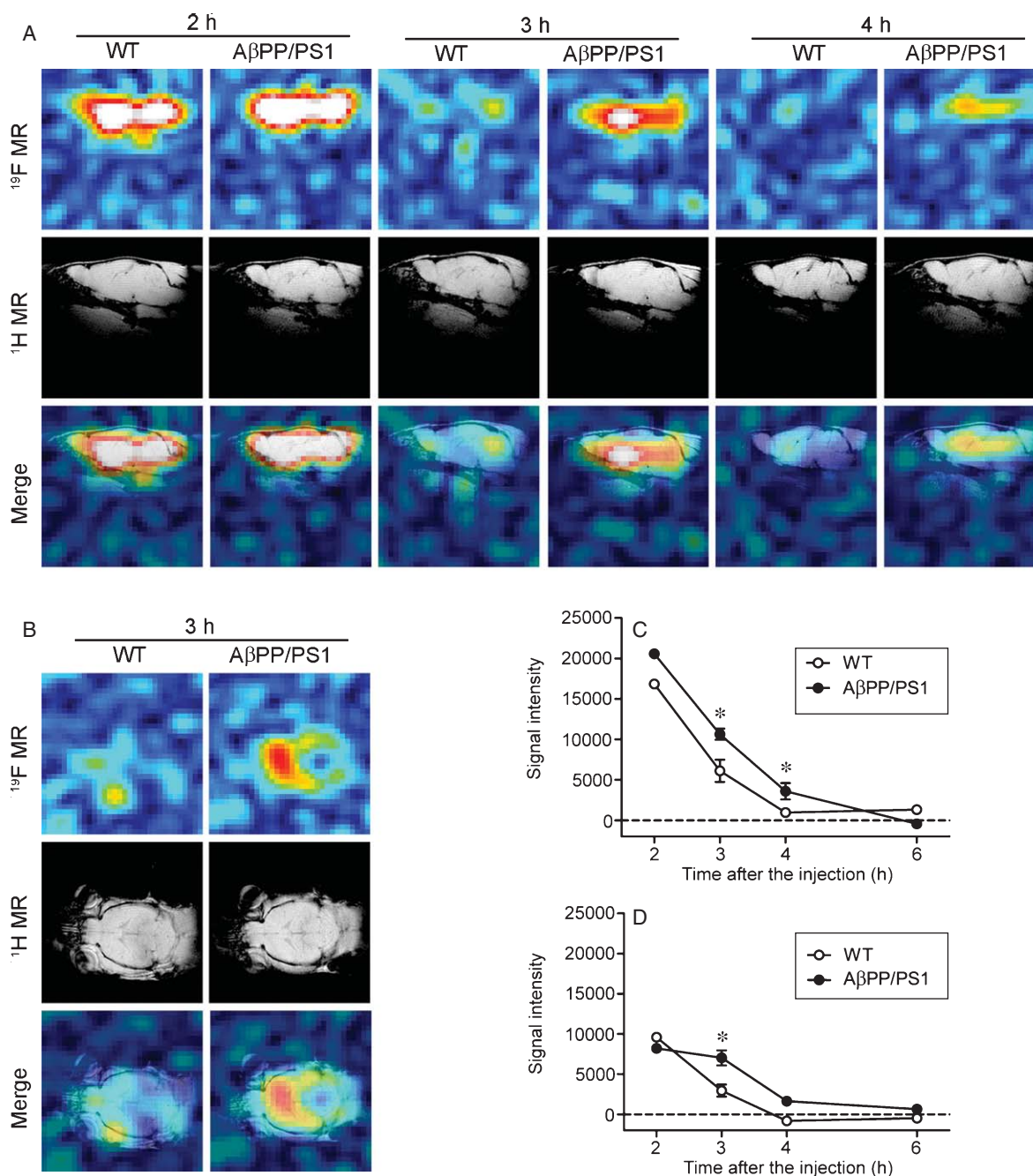


Fig. 2. Time course of changes in fluorine-19 magnetic resonance (^{19}F MR) signals in compound 3b ($m=6$)-injected 16- to 18-month-old wild-type (WT) and A β PPswe/PS1E9 double-transgenic (A β PP/PS1) mice. Mice were euthanized 2, 3, 4, or 6 h after the injection of probes. Subsequently, ^{19}F MR images were measured for 300 min in the sagittal plane (A) and horizontal plane (B). Relative signal intensities in the brain in the sagittal plane (C) and the horizontal plane (D) were calculated and plotted. In the sagittal plane, $n=1, 3, 3,$ and 1 WT mice and $n=1, 3, 4,$ and 1 A β PP/PS1 mice were imaged 2, 3, 4, and 6 h post-injection, respectively; in the horizontal plane, $n=1, 3, 1,$ and 1 WT mice and $n=1, 3, 2,$ and 2 A β PP/PS1 mice were imaged 2, 3, 4, and 6 h post-injection, respectively. Data are presented as mean \pm standard error of the mean (S.E.M.). Significance (Mann–Whitney test): * $p < 0.05$ versus WT.

not obtained, because 3 out of 3 mice died within 1 h post-injection. In mice injected with compound 5b ($m+n=10$) (Fig. 1) and compound 5b ($m+n=12$)

(data not shown), the ^{19}F MR signal was hardly detectable in the brain. In addition, *ex vivo* labeling with intravenously injected compound 5b ($m+n=10$)

and compound 5b ($m + n = 12$) showed far weaker signals in A β PP/PS1 mice, although intense spots were also detected in some of the plaques (Supplementary Figure 1). Taken together, these results suggest that the optimum number of ethylene glycol groups in the PEG chain to link with the fluorine-labeled group is seven.

Next, we tried to find out the best of the three types of trifluoromethyl groups (a, b, or c). We measured the ^{19}F MR signals of the 3',5'-bis(trifluoromethyl) benzylamino derivatives (6 fluorine atoms; type a). No remarkable differences were detected between A β PP/PS1 mice and wild-type mice for compounds 3a ($m = 4$) and 3a ($m = 5$). These compounds could be incorporated in adipose tissue in the orbit rather than the brain. We further tested the hexafluoroisopropoxy derivatives (6 fluorine atoms; type c). However, compounds 3c ($m = 6$) and 5c ($m + n = 8$) could not be solubilized enough in the micelle of Tween 80 to be intravenously injected, so ^{19}F MR data could not be obtained for these compounds.

We expected that the compounds containing two trifluoromethyl groups (6 fluorine atoms; type a and c) would give stronger ^{19}F MR signals than those containing one trifluoromethyl group (3 fluorine atoms; type b) in the brain of A β PP/PS1 mice. However, the above results suggested that increasing the number of trifluoromethyl groups would not necessarily be an effective way to make the ^{19}F MR signal stronger. Based on these observations, we selected compound 3b ($m = 6$) (Scheme 1C) as a candidate ^{19}F MRI probe for amyloid detection, and investigated it in the next part of the study. In addition, we chose 10% Tween 80 as the solubilizing agent for compound 3b ($m = 6$) because of the lower background level. The ^{19}F MR signal results of the probes we synthesized in the present study are summarized in Table 2.

Time course of changes in ^{19}F MR signal for compound 3b ($m = 6$)

We next investigated the time course of changes in the ^{19}F MR signals for compound 3b ($m = 6$) in 16- to 18-month-old A β PP/PS1 and wild-type mice. The mice were euthanized at various time points (2, 3, 4, and 6 h) after the injection of compound 3b ($m = 6$) dissolved in 10% Tween 80. Subsequently, ^{19}F MR signals were measured in the mouse head in the horizontal and sagittal planes for 300 min. In the sagittal plane, $n = 1, 3, 3,$ and 1 wild-type mice and $n = 1, 3, 4,$ and 1 A β PP/PS1 mice were imaged 2, 3, 4, and 6 h post-injection, respectively; in the horizontal plane,

Table 2

Summary of the results of fluorine-19 magnetic resonance (^{19}F MR) imaging using the probes we synthesized in the present study

Length of PEG (m, m + n)	Type of trifluoromethyl group		
	3a, 5a	3b, 5b	3c, 5c
2			
3			
4	(1)	(2)	
5	(1)	(2)	
6		(3)	(6)
7		(4)	
8		(4)	(6)
9			
10		(5)	
11			
12		(5)	

(1) No significant differences in the ^{19}F MR signals between A β PPswe/PS1dE9 double transgenic (A β PP/PS1) mice and wild-type mice were detected. (2) There were strong ^{19}F MR signals in the brain of A β PP/PS1 mice, compared with wild-type mice. (3) Intense ^{19}F MR signal was detected in the brain of A β PP/PS1 mice which was more prominent than (2). (4) Mice died after the injection. (5) No ^{19}F MR signal was detected in either A β PP/PS1 mice or wild-type mice. (6) There was difficulty dissolving the compounds for intravenous injection.

$n = 1, 3, 1,$ and 1 wild-type mice and $n = 1, 3, 2,$ and 2 A β PP/PS1 mice were imaged 2, 3, 4, and 6 h post-injection, respectively.

In the sagittal plane, strong ^{19}F MR signals were detected in the brain of both A β PP/PS1 mice and wild-type mice 2 h after injection (Fig. 2A). Although the ^{19}F MR signals in the wild-type mice readily decreased in a time-dependent manner, sizeable ^{19}F MR signals were still detected in the forebrain of A β PP/PS1 mice 3 and 4 h after injection (Fig. 2A). In a semi-quantitative analysis of the ^{19}F MR signal in the sagittal plane, ^{19}F MR signal intensity was significantly higher in the forebrain of A β PP/PS1 mice 3 and 4 h post-injection, compared to wild-type mice ($p < 0.05$; Fig. 2C). Significant ^{19}F MR signals were also detected in the forebrain of A β PP/PS1 mice in the horizontal plane 3 h post-injection ($p < 0.05$; Fig. 2B, D).

^{19}F MR measurement in living mice

We next measured the ^{19}F MR signals in living mice. A β PP/PS1 mice ($n = 3$) and wild-type mice ($n = 3$), aged 16 to 20 months, were placed in the MR scanner immediately after the end of the injection of compound 3b ($m = 6$). Then, a ^{19}F NMR spectrum was obtained from the whole head using a single pulse sequence for 10 min. Subsequently, ^{19}F CSI data for construction of ^{19}F MR images were collected from the head in the

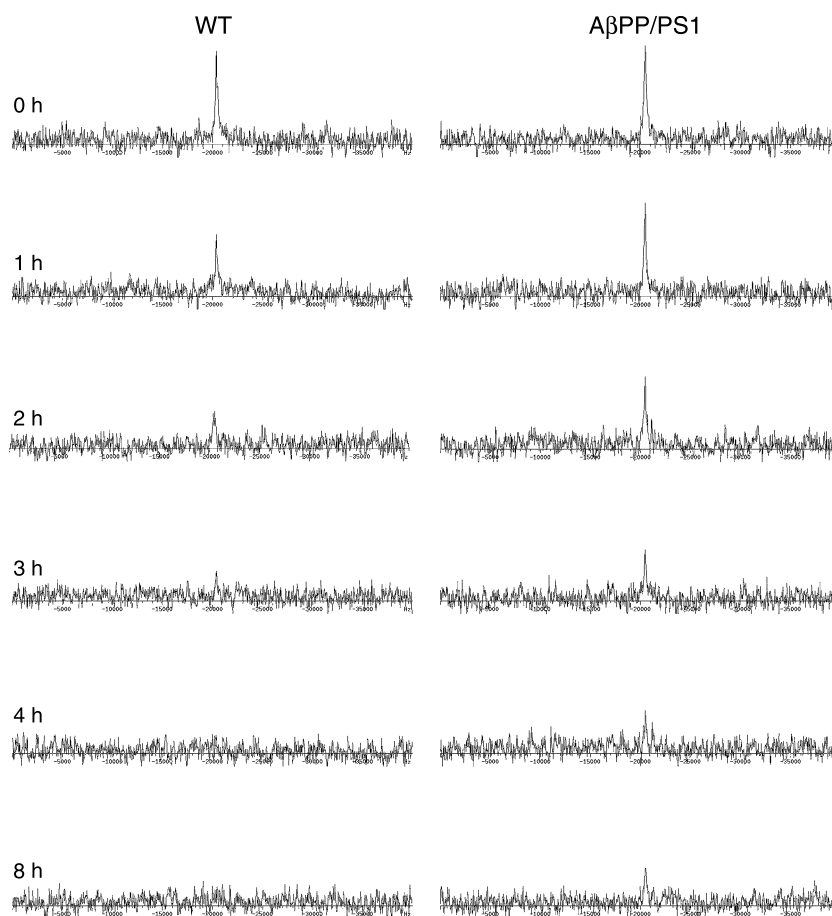


Fig. 3. Time course of changes in fluorine-19 nuclear magnetic resonance (^{19}F NMR) spectra in living 17- to 20-month-old wild-type (WT) and A β PPswe/PS1dE9 double-transgenic (A β PP/PS1) mice that were injected with compound 3b ($m = 6$). Panels show representative non-localized ^{19}F NMR spectra 0, 1, 2, 3, 4, and 8 h after intravenous injection of compound 3b ($m = 6$).

sagittal plane for 50 min. This set of MR measurements was repeated 7 times (a total of 8 sets).

In the ^{19}F NMR spectra, higher peaks were observed in A β PP/PS1 mice 1 h after injection and later, although there was no difference between wild-type mice and A β PP/PS1 mice immediately after the injection (Fig. 3). Then, although peaks in the wild-type mice were readily reduced by 3 h after injection, there remained substantial peaks in the A β PP/PS1 mice even at 8 h after injection.

In the ^{19}F MR images at the first measurement (10–60 min after injection of compound 3b [$m = 6$]), strong ^{19}F MR signals were observed in the brain of both wild-type mice and A β PP/PS1 mice (Fig. 4A). However, the signals in the brain of wild-type mice readily reduced with time. In contrast, strong ^{19}F MR signals were apparent in A β PP/PS1 mice 1–2 and 2–3 h post-injection, and still remained 3–4 h post-injection,

at which time the signal in wild-type mice had almost disappeared. We further compared ^{19}F MR images that were constructed by adding the data collected from 3 to 8 h after injection. The ^{19}F MR images clearly showed intense ^{19}F MR signals accumulated in the brain of A β PP/PS1 mice, while no signal was observed in wild-type mice (Fig. 4B). In addition, we measured ^{19}F MR images in A β PP/PS1 mice at 14 to 15 months of age ($n = 3$); however, no significant ^{19}F MR signals were apparent, compared with wild-type mice (Supplementary Figure 2).

Distribution pattern of amyloid deposits and ex vivo labeling with compound 3b ($m = 6$)

After the MR measurements, we prepared brain sections to investigate the distribution pattern of amyloid deposits and *ex vivo* labeling of plaques with

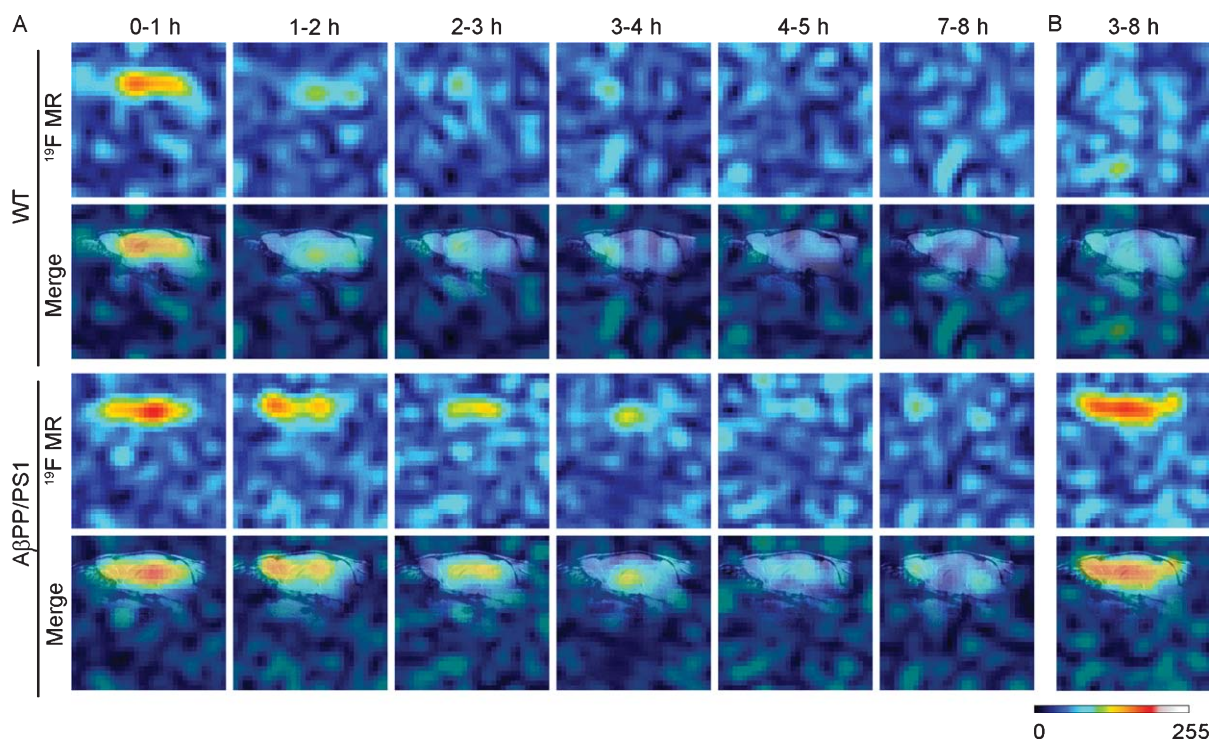


Fig. 4. Time course of changes in fluorine-19 magnetic resonance (^{19}F MR) signals in living 16- to 20-month-old wild-type (WT) and A β PPswe/PS1E9 double transgenic (A β PP/PS1) mice that were injected with compound 3b (m=6). A) Representative ^{19}F MR images were obtained for 50 min at 0, 1, 2, 3, 4, and 7 h after the intravenous injection of compound 3b (m=6). B) Representative ^{19}F MR images were constructed by adding the data collected from 3 h to 8 h after the intravenous injection of compound 3b (m=6).

intravenously injected compound 3b (m=6). Fluorescence microscopy revealed massive punctate fluorescence for compound 3b (m=6) in the cerebral cortex, hippocampus, and cerebellum in A β PP/PS1 mice (Fig. 5). In addition, most of the fluorescence was colocalized with the A β immunoreactivity. In contrast, no fluorescence for compound 3b (m=6) or A β immunoreactivity was apparent in wild-type mice.

Labeling with compound 3b (m=6) in human AD brain sections

Fluorescence microscopic analysis showed intense signal of compound 3b (m=6) that was colocalized with consolidated A β plaques in the temporal lobe (Fig. 6). In contrast, fluorescence signal of compound 3b (m=6) was not detected in AT8-immunoreactive paired helical filament in human AD brain (Fig. 6).

DISCUSSION

In the present study, we compared ^{19}F MR signals of fluorine-labeled compounds with PEG chains of dif-

fering numbers of ethylene glycol groups in the mouse brain. The results suggested that compound 3b (m=6), which bears a trifluoroethoxy group with seven ethylene glycol groups in the PEG chain, could be a useful ^{19}F MRI probe for amyloid detection in the brain.

The probes we synthesized in the present study consisted of styrylbenzoxazole as a core structure linked to the fluorine-labeled group by differing lengths of PEG chain. Styrylbenzoxazole is known as an amyloidophilic group, and its derivatives, such as BF-168, can bind to amyloid plaques in the living mouse brain after intravenous injection [22, 23]. In addition, *in vitro* fluorescence staining of compound 3b (m=6) in human AD brain sections showed high binding activity to senile plaques, and far less to neurofibrillary tangles. We used a PEG chain as a linker between the core structure and the fluorine-labeled group, and increasing the number of ethylene glycol groups in the PEG chain increases the hydrophilicity of the probes. In addition, using a PEG chain allows us to investigate the optimal distance between the core structure and the fluorine-labeled group, such that enough space is available to avoid inhibiting molecular mobility in the ^{19}F atoms

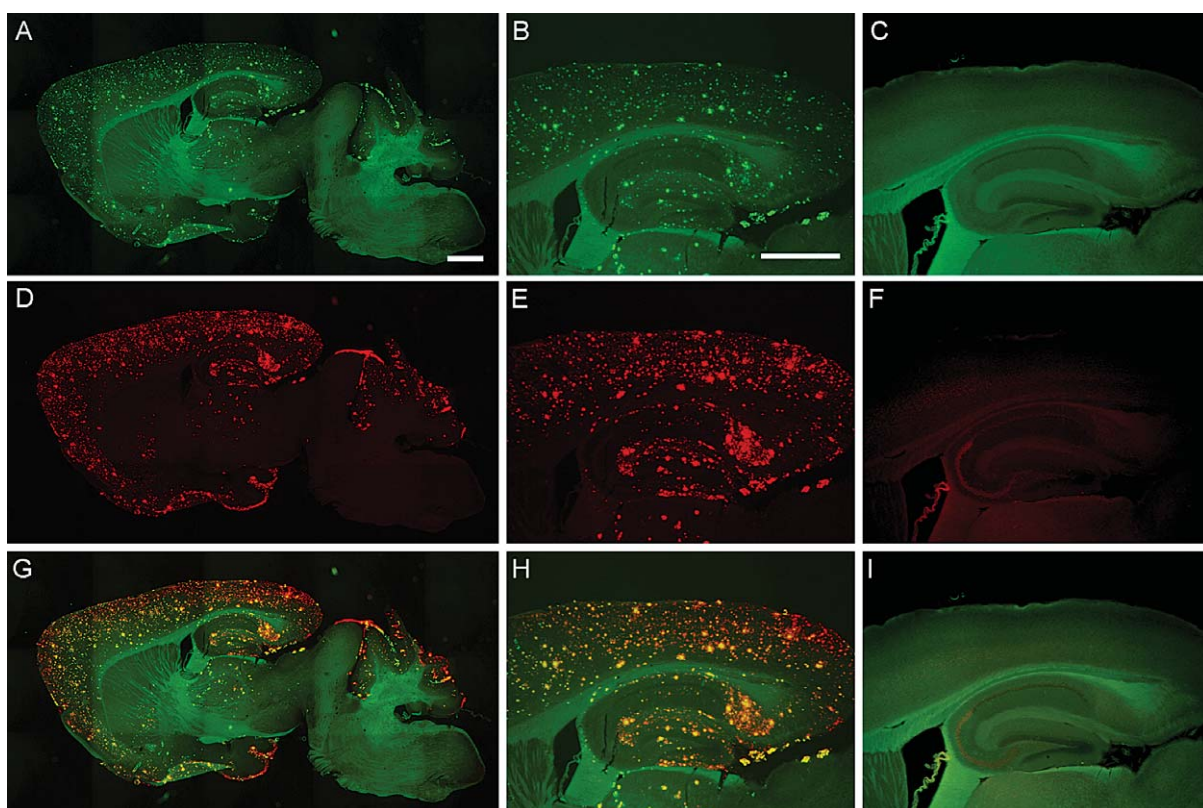


Fig. 5. Distribution pattern of amyloid deposits and *ex vivo* labeling with compound 3b ($m=6$). Representative images show fluorescence microscopic analysis in sagittal brain sections of A β PPswe/PS1dE9 double-transgenic mice (A, B, D, E, G, H) and wild-type mice (C, F, I) that received an intravenous injection of compound 3b ($m=6$). Fluorescence of compound 3b ($m=6$) and immunoreactivity for amyloid- β is shown as green (A–C) and red (D–F), respectively. Merged images (G–I). Scale bars are 1 mm (A, B).

when they bind to amyloid plaques. Our results showed that compound 3b ($m=6$), which has a trifluoroethoxy group with 7 ethylene glycol groups in the PEG chain, provided a remarkable ^{19}F MR signal in A β PP/PS1 mouse brains, but not in wild-type mouse brains. The compounds bearing shorter PEG chains ($m=2, 3$ and 4) showed a weak level of ^{19}F MR signal, suggesting a PEG chain of insufficient length to avoid the reduction in MR signal when bound to amyloid plaques in the brain. The compounds bearing eight and nine ethylene glycol groups in the PEG chain ($m+n=7$ and 8) proved fatal, although the cause of death was unclear. The compounds having longer PEG chains ($m+n=10$ and 12) showed no signals in the brain, probably because they are too large to penetrate the blood-brain barrier, which is supported by our findings of *ex vivo* labeling (Supplementary Figure 1). Based on these results, we concluded that seven ethylene glycol groups is the best length for the PEG chain to avoid the reduction in MR signal when the probe is bound to amyloid plaques.

This indicates that at least seven ethylene glycol groups are necessary for free mobility between the fluorinated group and the core structure that binds to the senile plaques in the brain.

In an *in vitro* study, increasing the number of fluorine atoms in the probe enabled us to detect higher NMR signal. However the hydrophobicity of the fluorine probe increases with the number of fluorine atoms, inducing an interaction with the membrane lipid in the brain [6, 20]. Thus, increasing the number of fluorine atoms in the probe would be an inappropriate way to develop a highly sensitive probe. Furthermore, to achieve high-sensitivity detection, the optimal functional group containing the fluorine atoms should be selected carefully since that group would crucially affect the level of ^{19}F MR signal in the brain *in vivo*. Taken together, these findings confirmed that compound 3b ($m=6$), which has seven ethylene glycol groups in the PEG chain as a linker with the trifluoroethoxy group, would be the optimal probe for

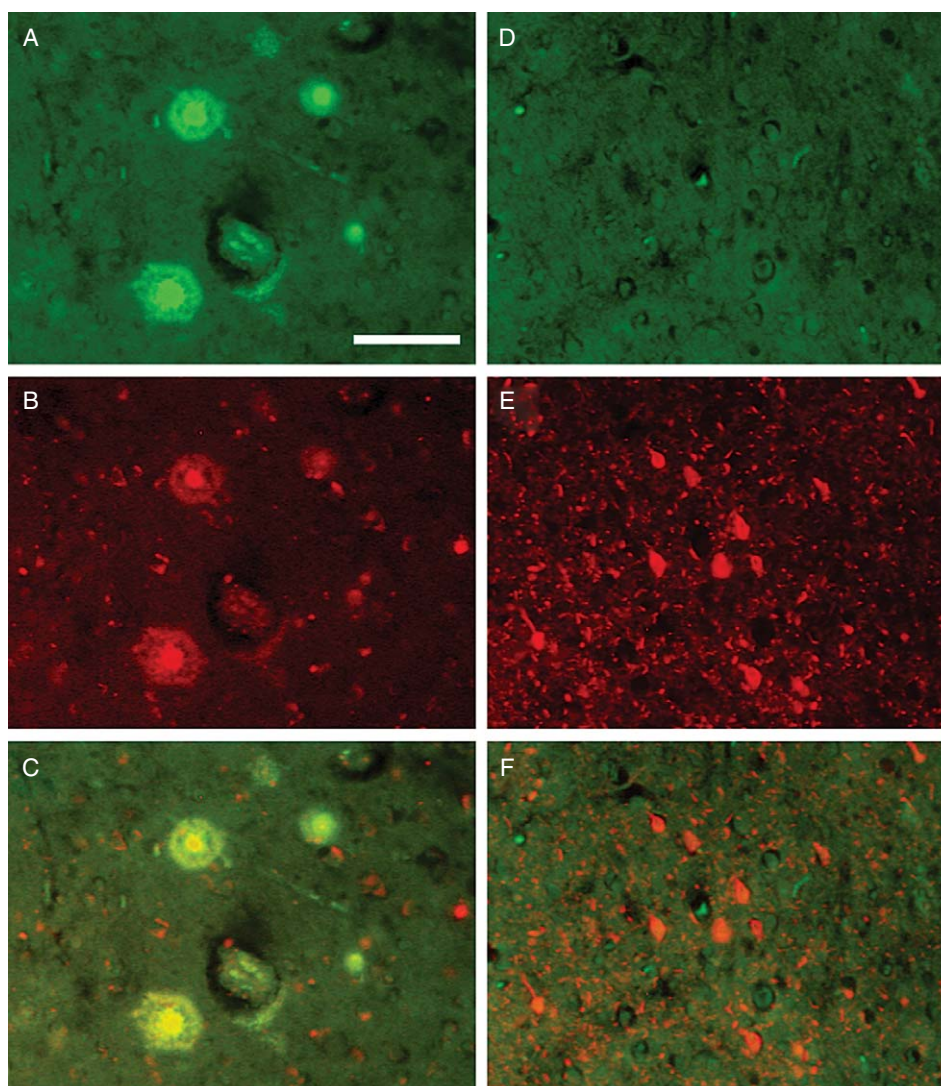


Fig. 6. Labeling with compound 3b ($m=6$) in human Alzheimer's disease (AD) brain sections. Representative images show fluorescence microscopic analysis in the temporal lobe sections of AD brain. Fluorescence of compound 3b ($m=6$) and immunoreactivity for amyloid- β (6E10) and phosphorylated tau (AT8) is shown as green (A, D) and red (B, E), respectively. Merged images (C, F). Scale bar: 100 μm (A).

maintaining a robust MR signal when bound to amyloid plaques. This finding is supported by the result that a strong ^{19}F MR signal was detected in the brain of compound 3b ($m=6$)-injected A β PP/PS1 mice that were perfused with saline 3 h post-injection (Supplementary Figure 3).

In the present study we used two surfactants, Tween 80 and Cremophor EL, to dissolve the probes for intravenous injection. The results showed intense ^{19}F MR signals in both the A β PP/PS1 and wild-type mouse brains with compound 3b ($m=6$) dissolved in 10% Cremophor EL. In contrast, compound 3b

($m=6$) dissolved in 10% Tween 80 showed strong ^{19}F MR signals only in A β PP/PS1 mice, and little signal in wild-type mice, indicating a significant difference between A β PP/PS1 mice and wild-type mice. Therefore, we used 10% Tween 80 as a solubilizing agent for compound 3b ($m=6$). In our preliminary study, the decreasing rate of ^{19}F MR signal from the head became slower when the compounds were injected in 10% Cremophor EL. Thus, the solubilizing agent is another key factor, because it appears to change the distribution or metabolism of the probe, and thus affects ^{19}F MR signals.

We detected a remarkable ^{19}F MR signal in the brain of living A β PP/PS1 mice over 17 months of age after injection of compound 3b ($m = 6$). The brain region in which ^{19}F MR signals were detected was in accordance with the distribution pattern of amyloid deposits in the brain of A β PP/PS1 mice. In contrast, the ^{19}F MR signal was slightly, but not obviously, apparent in the brain of living 14-month-old A β PP/PS1 mice that had already developed moderate amyloid deposits in the brain (Supplementary Figure 4). Immunohistochemical analysis of A β PP/PS1 mice at 20 months of age showed high levels of amyloid deposition in the brain, compared with that at 14 months of age (Supplementary Figure 4). Thus, the level of ^{19}F MR signal detected by our method would depend on the level of amyloid deposition in the brain, and sensitivity would need to be improved to detect amyloid deposition in younger A β PP/PS1 mice.

We did not determine the bioavailability and toxicity of the compounds in the present study. A study by Okamura et al. showed that the ^{18}F -radiolabeled styrylbenzoxazole derivative, BF-168, displayed ideal kinetic properties, including abundant initial brain uptake (3.9% of the injected dose per gram at 2 min after injection) and a short clearance half-life (24.7 min) in normal mouse brain, although some persistence of BF-168 or its metabolites remained in the plasma over 1 h after the injection [23]. Thus, while detailed investigations are still needed, we believe that our styrylbenzoxazole compounds also show good bioavailability to image amyloid deposition in the brain. On the other hand, the toxicity of the compounds has not been elucidated. Compounds 5b ($m + n = 7$ and 8) bearing eight and nine ethylene glycol groups in the PEG chain, respectively, proved fatal, implying that the compounds used in the present study have potential toxicity. However we found no obvious sign of toxicity in the central nervous system or peripheral organs in mice following injections of compound 3b ($m = 6$) and others, except for compounds 5b ($m + n = 7$ and 8). Therefore although further study is still needed, we consider that compound 3b ($m = 6$) shows very low toxicity.

Currently, PET is used as a powerful imaging modality to detect amyloid deposition. PET has great advantages including excellent sensitivity, the very low doses required, and high quantitative ability, compared to other imaging modalities. However, it suffers from some drawbacks, including limited spatial resolution, the need to manipulate radioactive compounds, and the high cost and the narrow availability of radioisotopes for PET probes as well as the low availability of

PET scanners for preclinical studies in animals. Thus, alternative methods based on other imaging modalities, such as MRI, are currently being developed to detect amyloid plaques. MRI would offer several advantages over PET because MRI provides better spatial resolution, is more widely available, is less costly, and lacks radiation exposure as compared to PET.

Recent studies demonstrated that individual amyloid plaques in AD model mice are detectable as hypointense spots in T2- and T2*-weighted ^1H MR images from a high field MR scanner [7, 8, 10, 11]. In this case, it is likely that the hypointense spots based on the reduction in T2 are induced by accumulation of metals such as iron in the amyloid plaques and/or by other factors such as the dense structure of the plaques. However, the number of spots visualized by intrinsic MRI is far less than the number of plaques seen in histological analysis. In addition, this method is not specific for amyloid plaques because it also detects other iron-containing structures such as remnants of old hemorrhages and calcification. On the other hand, several contrast agents are being developed to enhance the detectability of plaques in ^1H MRI, such as Gd- or UPIO-labeled amyloid binding agent [13, 17]. This imaging method is able to detect more amyloid plaques with increasing signal-to-noise ratio and contrast-to-noise ratio. However, use of a technique to induce transient blood-brain barrier opening to deliver the contrast agent into the brain is needed to visualize amyloid plaques in MRI, since these contrast agents do not readily cross the blood-brain barrier. Therefore, in this context and according to the advantages mentioned in the Introduction, our ^{19}F MRI technique could be a potential alternative imaging technique for evaluating amyloid deposition. For clinical applications, we need to modify the methodology to overcome several problems, such as the high dose required for imaging and the low sensitivity and resolution.

In the present study, we investigated the preferred features of a ^{19}F MRI probe for amyloid detection in the brain, and found compound 3b ($m = 6$) to be the best candidate. This compound has seven ethylene glycol groups in the PEG chain as a linker between the core structure and the trifluoroethoxy group. Compound 3b ($m = 6$) showed strong ^{19}F MR signals in the brain where massive amyloid deposition was detected, suggesting that the probes could generate a high level of ^{19}F MR signal when bound to amyloid plaques in the brain. Thus, this study has identified the optimum length of PEG chain and appropriate fluorine-labeled group for a probe to generate a strong MR signal for amyloid imaging with ^{19}F MRI.

ACKNOWLEDGMENTS

The authors thank Ms. Takako Sasamura for her excellent technical assistance. This study was supported by Grant-in-Aids for Scientific Research (B) (JSPS KAKENHI Grant Number 22300153) (I.T.) and for Young Scientists (B) (25750159) (D.Y.) from the Japan Society for the Promotion of Science (JSPS), and a Grant-in-Aid for Scientific Research on Innovative Areas (“Brain Environment”) (MEXT KAKENHI Grant Number 24111522) (I.T.) from the Ministry of Education, Science, Sports and Culture of Japan (MEXT).

Authors’ disclosures available online (<http://www.j-alz.com/disclosures/view.php?id=1976>).

SUPPLEMENTARY MATERIAL

Supplementary material is available in the electronic version of this article: <http://dx.doi.org/10.3233/JAD-131025>.

REFERENCES

- [1] Citron M (2010) Alzheimer’s disease: Strategies for disease modification. *Nat Rev Drug Discov* **9**, 387-398.
- [2] Querfurth HW, LaFerla FM (2010) Alzheimer’s disease. *N Engl J Med* **362**, 329-344.
- [3] Hardy J, Selkoe DJ (2002) The amyloid hypothesis of Alzheimer’s disease: Progress and problems on the road to therapeutics. *Science* **297**, 353-356.
- [4] Jack CR Jr, Knopman DS, Jagust WJ, Shaw LM, Aisen PS, Weiner MW, Petersen RC, Trojanowski JQ (2010) Hypothetical model of dynamic biomarkers of the Alzheimer’s pathological cascade. *Lancet Neurol* **9**, 119-128.
- [5] Sperling RA, Aisen PS, Beckett LA, Bennett DA, Craft S, Fagan AM, Iwatsubo T, Jack CR Jr, Kaye J, Montine TJ, Park DC, Reiman EM, Rowe CC, Siemers E, Stern Y, Yaffe K, Carrillo MC, Thies B, Morrison-Bogorad M, Wagster MV, Phelps CH (2011) Toward defining the preclinical stages of Alzheimer’s disease: Recommendations from the National Institute on Aging-Alzheimer’s Association workgroups on diagnostic guidelines for Alzheimer’s disease. *Alzheimer’s Dement* **7**, 280-292.
- [6] Amatsubo T, Yanagisawa D, Morikawa S, Taguchi H, Tooyama I (2010) Amyloid imaging using high-field magnetic resonance. *Magn Reson Med Sci* **9**, 95-99.
- [7] Benveniste H, Einstein G, Kim KR, Hulette C, Johnson GA (1999) Detection of neuritic plaques in Alzheimer’s disease by magnetic resonance microscopy. *Proc Natl Acad Sci U S A* **96**, 14079-14084.
- [8] Chamberlain R, Reyes D, Curran GL, Marjanska M, Wengenack TM, Poduslo JF, Garwood M, Jack CR, Jr. (2009) Comparison of amyloid plaque contrast generated by T2-weighted, T2*-weighted, and susceptibility-weighted imaging methods in transgenic mouse models of Alzheimer’s disease. *Magn Reson Med* **61**, 1158-1164.
- [9] Higuchi M, Iwata N, Matsuba Y, Sato K, Sasamoto K, Saido TC (2005) ¹⁹F and ¹H MRI detection of amyloid beta plaques *in vivo*. *Nat Neurosci* **8**, 527-533.
- [10] Jack CR Jr, Garwood M, Wengenack TM, Borowski B, Curran GL, Lin J, Adriany G, Gröhn OH, Grimm R, Poduslo JF (2004) *In vivo* visualization of Alzheimer’s amyloid plaques by magnetic resonance imaging in transgenic mice without a contrast agent. *Magn Reson Med* **52**, 1263-1271.
- [11] Jack CR Jr, Wengenack TM, Reyes DA, Garwood M, Curran GL, Borowski BJ, Lin J, Preboske GM, Holasek SS, Adriany G, Poduslo JF (2005) *In vivo* magnetic resonance microimaging of individual amyloid plaques in Alzheimer’s transgenic mice. *J Neurosci* **25**, 10041-10048.
- [12] Petiet A, Santin M, Bertrand A, Wiggins CJ, Petit F, Houitte D, Hantraye P, Benavides J, Debeir T, Rooney T, Dhenain M (2012) Gadolinium-staining reveals amyloid plaques in the brain of Alzheimer’s transgenic mice. *Neurobiol Aging* **33**, 1533-1544.
- [13] Poduslo JF, Wengenack TM, Curran GL, Wisniewski T, Sigurdsson EM, Macura SI, Borowski BJ, Jack CR Jr (2002) Molecular targeting of Alzheimer’s amyloid plaques for contrast-enhanced magnetic resonance imaging. *Neurobiol Dis* **11**, 315-329.
- [14] Sigurdsson EM, Wadghiri YZ, Mosconi L, Blind JA, Knudsen E, Asuni A, Scholtzova H, Tsui WH, Li Y, Sadowski M, Turnbull DH, de Leon MJ, Wisniewski T (2008) A non-toxic ligand for voxel-based MRI analysis of plaques in AD transgenic mice. *Neurobiol Aging* **29**, 836-847.
- [15] Wadghiri YZ, Sigurdsson EM, Sadowski M, Elliott JI, Li Y, Scholtzova H, Tang CY, Aguinaldo G, Pappolla M, Duff K, Wisniewski T, Turnbull DH (2003) Detection of Alzheimer’s amyloid in transgenic mice using magnetic resonance microimaging. *Magn Reson Med* **50**, 293-302.
- [16] Wengenack TM, Reyes DA, Curran GL, Borowski BJ, Lin J, Preboske GM, Holasek SS, Gilles EJ, Chamberlain R, Marjanska M, Jack CR Jr, Garwood M, Poduslo JF (2011) Regional differences in MRI detection of amyloid plaques in AD transgenic mouse brain. *Neuroimage* **54**, 113-122.
- [17] Yang J, Wadghiri YZ, Hoang DM, Tsui W, Sun Y, Chung E, Li Y, Wang A, de Leon M, Wisniewski T (2011) Detection of amyloid plaques targeted by USPIO-Aβ 1-42 in Alzheimer’s disease transgenic mice using magnetic resonance microimaging. *Neuroimage* **55**, 1600-1609.
- [18] Amatsubo T, Morikawa S, Inubushi T, Urushitani M, Taguchi H, Shirai N, Hirao K, Kato M, Morino K, Kimura H, Nakano I, Yoshida C, Okada T, Sano M, Tooyama I (2009) Trifluoromethoxy-benzylated ligands improve amyloid detection in the brain using ¹⁹F magnetic resonance imaging. *Neurosci Res* **63**, 76-81.
- [19] Yanagisawa D, Shirai N, Amatsubo T, Taguchi H, Hirao K, Urushitani M, Morikawa S, Inubushi T, Kato M, Kato F, Morino K, Kimura H, Nakano I, Yoshida C, Okada T, Sano M, Wada Y, Wada K, Yamamoto A, Tooyama I (2010) Relationship between the tautomeric structures of curcumin derivatives and their Aβ-binding activities in the context of therapies for Alzheimer’s disease. *Biomaterials* **31**, 4179-4185.
- [20] Yanagisawa D, Amatsubo T, Morikawa S, Taguchi H, Urushitani M, Shirai N, Hirao K, Shiino A, Inubushi T, Tooyama I (2011) *In vivo* detection of amyloid β deposition using ¹⁹F magnetic resonance imaging with a ¹⁹F-containing curcumin derivative in a mouse model of Alzheimer’s disease. *Neuroscience* **184**, 120-127.
- [21] Jankowsky JL, Fadale DJ, Anderson J, Xu GM, Gonzales V, Jenkins NA, Copeland NG, Lee MK, Younkin LH, Wagner

- SL, Younkin SG, Borchelt DR (2004) Mutant presenilins specifically elevate the levels of the 42 residue beta-amyloid peptide *in vivo*: Evidence for augmentation of a 42-specific gamma secretase. *Hum Mol Genet* **13**, 159-170.
- [22] Kudo Y, Okamura N, Furumoto S, Tashiro M, Furukawa K, Maruyama M, Itoh M, Iwata R, Yanai K, Arai H (2007) 2-(2-[2-Dimethylaminothiazol-5-yl]ethenyl)-6-(2-[fluoro]ethoxy)benzoxazole: A novel PET agent for *in vivo* detection of dense amyloid plaques in Alzheimer's disease patients. *J Nucl Med* **48**, 553-561.
- [23] Okamura N, Suemoto T, Shimadzu H, Suzuki M, Shiomitsu T, Akatsu H, Yamamoto T, Staufenbiel M, Yanai K, Arai H, Sasaki H, Kudo Y, Sawada T (2004) Styrylbenzoxazole derivatives for *in vivo* imaging of amyloid plaques in the brain. *J Neurosci* **24**, 2535-2541.